Estimation of interval anisotropic attenuation from reflection data

Jyoti Behura & Ilya Tsvankin
Center for Wave Phenomena, Geophysics Department, Colorado School of Mines, Golden, Colorado 80401

ABSTRACT
Knowledge of interval attenuation can be highly beneficial in reservoir characterization and lithology discrimination. Here, we combine the spectral-ratio method with velocity-independent layer-stripping to develop a technique for estimation of the interval phase attenuation coefficient from reflection seismic data. The algorithm is designed for arbitrarily anisotropic target layers, but the overburden is assumed to be laterally homogeneous with a horizontal symmetry plane. Although no velocity information about the overburden is needed, interpretation of the anisotropic attenuation coefficient in the target layer requires estimation of the velocity function.
The interval phase attenuation in a reservoir can be used to predict the presence and distribution of hydrocarbons. For example, our method can help to distinguish between steam and heat fronts in heavy-oil reservoirs. Azimuthal variation of the interval attenuation in fractured formations can provide sensitive attributes for fracture characterization and reconstruction of the stress field.

Key words: Attenuation anisotropy, interval attenuation, spectral-ratio method, layer stripping

1 INTRODUCTION

Attenuation analysis can provide valuable information about lithology and physical properties of subsurface rocks. Laboratory measurements (e.g., Winkler & Nur, 1982) show that attenuation is closely related to the presence of fluids. In particular, attenuation may serve as an indicator of permeability, mobility of fluids, and fluid saturation (e.g., Batzle *et al.*, 2006; Behura *et al.*, 2007).

A number of laboratory measurements (Behura *et al.*, 2006; Hosten *et al.*, 1987; Prasad & Nur, 2003; Tao & King, 1990) and field case studies (Ganley & Kanasewich, 1980; Liu *et al.*, 2007; Maultzsch *et al.*, 2007) indicate that attenuation can be strongly anisotropic (directionally-dependent) because of the preferential alignment of fractures, interbedding of thin attenuative layers, and nonhydrostatic stress. The field study of Maultzsch *et al.* (2007) finds the symmetry of attenuation anisotropy to be different from that of velocity anisotropy. Therefore, measurements of attenuation anisotropy may provide additional information about the fluid properties of fractured reservoirs (Liu *et al.*, 2007).

Existing attenuation estimates from reflection data (e.g., Vasconcelos & Jenner, 2005) are obtained for the whole section above the reflecting interface. Dasgupta & Clark (1998) introduce a technique for estimating interval attenuation from reflection data based on the spectral ratio method. This algorithm, however, is restricted to zero-offset attenuation and requires the knowledge of the source signature. Moreover, they apply the NMO stretch prior to attenuation analysis, which may distort the estimated attenuation values.

Here, we present a method for computing the *interval* attenuation coefficients using an extension of the layer-stripping technique originally introduced by Dewangan & Tsvankin (2006) for reflection traveltimes. Our algorithm reconstructs the offset-dependent interval attenuation of an arbitrarily anisotropic heterogeneous target layer without knowledge of the velocity and attenuation in the overburden. Synthetic examples for layered VTI (transversely isotropic with a verti-

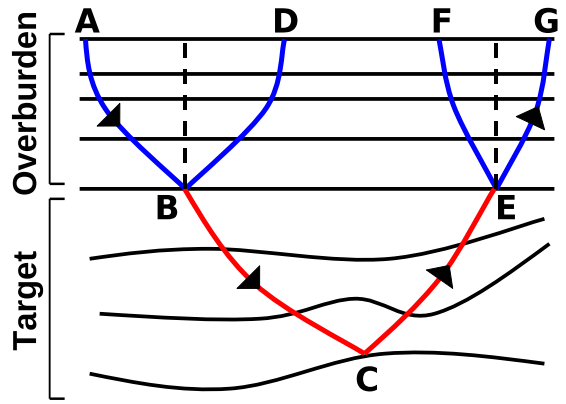

Figure 1. 2D ray diagram of the layer-stripping algorithm. Points B and E are located at the bottom of the overburden. The target reflection $ABCEG$ and the reflection ABD from the bottom of the overburden share the same downgoing leg AB. The upgoing leg of the target event EG coincides with a leg of another overburden reflection (GEF).

cal symmetry axis) media confirm the accuracy of our method and its potential in the inversion for the interval attenuation-anisotropy parameters.

2 METHODOLOGY

Although our technique of estimating interval attenuation can be applied in 3D, this work is restricted to 2D models. Let us consider a pure-mode reflection in a medium that consists of an anisotropic, heterogeneous target layer under a laterally homogeneous overburden with a horizontal symmetry plane (Figure 1). To make wave propagation two-dimensional, the vertical incidence plane has to be a plane of symmetry in all layers. This restriction can be relaxed in the 3D version of the method operating with wide-azimuth data.

The exact interval traveltime-offset function in the target layer can be constructed by combining the target event with reflections from the bottom of the overburden (Figure 1). Dewangan & Tsvankin (2006) show that by matching the time slopes (slownesses) on common-receiver gathers, it is possible to identify the overburden reflections ABD and GEF that share the downgoing (AB) and upgoing (EG) legs with the target event $ABCEG$. Under the assumptions made above, any reflection point at the bottom of the overburden (e.g., points B and E in Figure 1) coincides with the common midpoint for the corresponding source-receiver pair, and the traveltimes along the downgoing and upgoing segments of the reflected ray are equal to each other. Therefore, the interval traveltime in the target layer along the path BCE can be obtained by

$$t_{BCE} = t_{ABCEG} - \frac{t_{ABD} + t_{GEF}}{2}, \quad (1)$$

where t_{ABCEG}, t_{ABD}, and t_{GEF} are the traveltimes along the raypaths $ABCEG$, ABD, and GEF respectively.

Here, we extend this layer-stripping technique to attenuation analysis by applying the spectral-ratio method to the frequency-domain amplitudes of the target and overburden events. The amplitude of the overburden reflections can be written as

$$|U_{ABD}(\omega)| = S(\omega)\,\mathcal{G}_{ABD}\,e^{-k^I_{g,O}(l_{AB}+l_{BD})} \quad (2)$$

and

$$|U_{GEF}(\omega)| = S(\omega)\,\mathcal{G}_{GEF}\,e^{-k^I_{g,O}(l_{EG}+l_{EF})}, \quad (3)$$

while for the target reflection $|U_{ABCEG}(\omega)|$, we have

$$|U_{ABCEG}(\omega)| = S(\omega)\,\mathcal{G}_{ABCEG}\,e^{-k^I_{g,O}(l_{AB}+l_{EG})}\,e^{-k^I_{g,T}(l_{BC}+l_{CE})}, \quad (4)$$

where $S(\omega)$ is the spectrum of the source wavelet, l_{XY} represents the distance along the raypath XY; $k^I_{g,T}$ and $k^I_{g,O}$ ("I" stands for the imaginary part of the wavenumber) are the average group attenuation coefficients in the target layer and overburden, respectively, and the parameters $\mathcal{G}_{ABD}$, $\mathcal{G}_{GEF}$, and $\mathcal{G}_{ABCEG}$ include the source/receiver radiation patterns as well as the reflection/transmission coefficients and geometrical spreading along the corresponding raypaths.

Then the interval attenuation coefficient in the target layer can be computed using the following combination of amplitudes:

$$ln\left(\frac{|U_{ABCEG}(\omega)|^2}{|U_{ABD}(\omega)|\,|U_{GEF}(\omega)|}\right) = ln(\mathcal{G}) - 2k^I_{g,T}(l_{BC}+l_{CE}) - 2k^I_{g,O}(l_{AB}-l_{BD}) - 2k^I_{g,O}(l_{EG}-l_{FE}), \quad (5)$$

where $\mathcal{G} = \mathcal{G}^2_{ABCEG}/(\mathcal{G}_{ABD}\mathcal{G}_{GEF})$. It is reasonable to assume that the term $\mathcal{G}$ is independent of frequency; note that the source wavelet in equation 5 has been eliminated. Because the overburden is laterally homogeneous and has a horizontal symmetry plane, $l_{AB} = l_{BD}$ and $l_{EG} = l_{FE}$. Then equation 5 reduces to

$$ln\left(\frac{|U_{ABCEG}(\omega)|^2}{|U_{ABD}(\omega)|\,|U_{GEF}(\omega)|}\right) = ln(\mathcal{G}) - 2k^I_{g,T}(l_{BC}+l_{CE}). \quad (6)$$

Therefore, application of equation 6 helps to remove the influence of the attenuation in the overburden.

For anisotropic attenuative media, the group attenuation coefficient k^I_g generally differs from the phase attenuation coefficient k^I. If the inhomogeneity angle (the angle between the real and imaginary parts of the complex wave vector) is small, the group and phase attenuation coefficients are related by $k^I_g = k^I \cos\psi$, where

ψ is the angle between the group- and phase-velocity vectors (Zhu, 2006).

For an arbitrarily heterogeneous target layer, the attenuation coefficient varies along the ray, and $k^I_{g,T}$ in equation 6 represents the average value along the ray-path BCE. However, if the target layer is horizontal, homogeneous, and has a horizontal symmetry plane (or is purely isotropic), then $l_{BC} + l_{CE} = V_g\, t_{BCE}$, where V_g is the group velocity. Then equation 6 can be written as

$$ln\left(\frac{|U_{ABCEG}(\omega)|^2}{|U_{ABD}(\omega)|\,|U_{GEF}(\omega)|}\right) \quad = \quad ln(\mathcal{G}) - 2\,k^I \cos\psi\, V_g\, t_{BCE}. \qquad (7)$$

Expressing V_g through the phase velocity V ($V_g = V/\cos\psi$), we represent the attenuation-related term in equation 7 as follows:

$$k^I \cos\psi\, V_g\, t_{BCE} \quad = \quad \omega\,\frac{k^I}{k}\,t_{BCE} \quad = \quad \omega\,\mathcal{A}\,t_{BCE}. \qquad (8)$$

$\mathcal{A} = k^I/k$ ($k = \omega/V$) is the normalized phase attenuation coefficient (Zhu & Tsvankin, 2006). Therefore, equation 7 can be rewritten as

$$ln\left(\frac{|U_{ABCEG}(\omega)|^2}{|U_{ABD}(\omega)|\,|U_{GEF}(\omega)|}\right) \quad = \quad ln(\mathcal{G}) - 2\,\omega\,\mathcal{A}\,t_{BCE}. \qquad (9)$$

In the above derivation, the inhomogeneity angle ξ (i.e., the angle between the real and imaginary parts of the wave vector) is assumed to be zero (Figure 2a). However, as discussed below, equation 9 remains valid for a wide range of inhomogeneity angles.

The slope of the logarithmic spectral ratio in equation 9 expressed as a function of ω yields the product $2\,\mathcal{A}\,t_{BCE}$. Since the interval traveltime t_{BCE} can be obtained from the layer-stripping algorithm (equation 1), equation 9 can be used to estimate the phase attenuation coefficient $\mathcal{A}$. To invert $\mathcal{A}$ for the attenuation-anisotropy parameters (Zhu *et al.*, 2007), it is necessary to estimate the phase direction. Since the influence of attenuation on velocity is typically of the second order (Zhu & Tsvankin, 2006), velocity analysis for the target layer can be performed prior to attenuation processing using the interval traveltime. Note that the inversion for the parameters of an anisotropic target layer typically requires *a priori* information (e.g., the layer thickness).

Computation of the interval values of $\mathcal{A}$ for different source-receiver pairs can help to evaluate both the anisotropy and lateral variation of attenuation. Although we described the methodology only for 2D models, it can be readily extended to 3D wide-azimuth data using the 3D version of the layer-stripping algorithm of Dewangan & Tsvankin (2006).

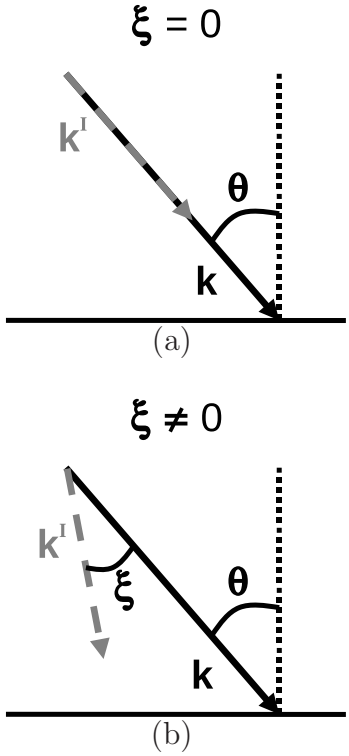

Figure 2. Incident plane wave with (a) zero inhomogeneity angle and (b) nonzero inhomogeneity angle ξ. $\mathbf{k}$ and $\mathbf{k}^I$ are the real and imaginary components (respectively) of the wave vector, and θ is the incidence phase angle.

3 SYNTHETIC EXAMPLE

The layer-stripping method introduced above was tested on synthetic PP-reflection data generated for a layered VTI model (Figure 3). A shot gather computed by an anisotropic reflectivity code is shown in Figure 4a. Note that the reflections from the bottom of the attenuative layers have much lower frequency content than the water-bottom event (Figure 4b).

Attenuation in VTI media can be conveniently characterized using the Thomsen-style notation ($\mathcal{A}_{P0} \approx 1/2Q_{P0}$, $\mathcal{A}_{S0} \approx 1/2Q_{S0}$, ϵ_Q, δ_Q, γ_Q) introduced by Zhu & Tsvankin (2006). $\mathcal{A}_{P0}$ and $\mathcal{A}_{S0}$ are the normalized symmetry-direction attenuation coefficients of the P- and S-waves, respectively, ϵ_Q and δ_Q control the angular variation of the P- and SV-wave attenuation coefficients, and γ_Q governs SH-wave attenuation anisotropy. Although the second layer has uncommonly strong attenuation ($Q_{P0} = 10$), the estimated interval attenuation coefficient is close to the exact values for a wide range of angles (Figure 5a). Attenuation coefficients for large phase angles (outside the range of $\pm 60^\circ$) are missing because of the limited acquisition aperture. The interval attenuation coefficient computed for the third layer (Figure 5b) is accurate only up to $\pm 30^\circ$. For phase angles exceeding 30°, the target reflection interferes

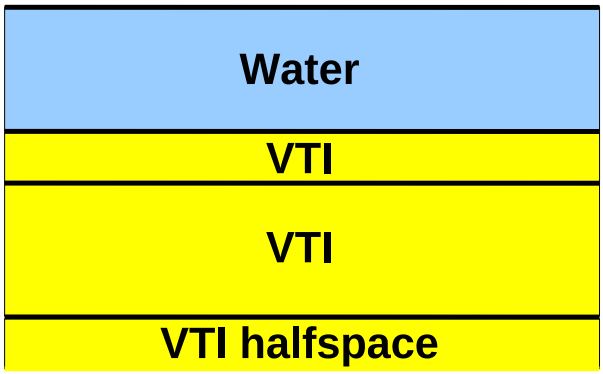

Figure 3. Model used to test the attenuation layer-stripping algorithm. The first layer is water (purely elastic and isotropic) with the P-wave velocity $V_P = 1500$ m/s and thickness $d = 1000$ m; the other three layers are VTI. For the second layer, the parameters are as follows: the vertical P- and S-wave velocities are $V_{P0} = 1600$ m/s and $V_{S0} = 200$ m/s, $d = 300$ m, and Thomsen velocity-anisotropy parameters are $\epsilon = 0.3$ and $\delta = -0.2$; the attenuation parameters are $Q_{P0} = 10$, $Q_{S0} = 10$, $\epsilon_Q = -0.5$, and $\delta_Q = -1.0$. The third layer has $V_{P0} = 2000$ m/s, $V_{S0} = 1000$ m/s, $d = 1000$ m, $\epsilon = 0.1$, $\delta = 0.6$, $Q_{P0} = 200$, $Q_{S0} = 200$, $\epsilon_Q = -0.3$, and $\delta_Q = 1.0$. For the bottom halfspace, $V_{P0} = 2200$ m/s, $V_{S0} = 1100$ m/s, $\epsilon = 0$, $\delta = -0.2$, $Q_{P0} = 100$, $Q_{S0} = 100$, $\epsilon_Q = 0.5$, and $\delta_Q = 0.5$.

with the direct arrival and other events, making the spectral-ratio method inadequate. Interference-related distortions can be mitigated by operating in the $\tau - p$ domain or suppressing the direct arrival and ground roll before layer stripping. This and other tests (not shown here) performed for a wide range of attenuative anisotropic models confirm the accuracy and efficiency of our method.

4 DISCUSSION

Although the above methodology is developed for zero inhomogeneity angle ξ (Figure 2a), our analysis supported by exact numerical modeling shows that it remains accurate for a wide range of ξ. Application of equations 7 and 8 for nonzero inhomogeneity angles yields the normalized phase attenuation coefficient $\mathcal{A}$ corresponding to $\xi = 0^\circ$. This conclusion remains valid even for large inhomogeneity angles ($\xi < 80^\circ$) and media with Q as low as 10. For this reason, the phase attenuation coefficient in off-symmetry directions in Figure 5 is computed accurately, even though the inhomogeneity angle reaches 45° for long offsets.

The attenuation-anisotropy parameters can be obtained by fitting the estimated interval phase attenuation coefficient to the following approximate expression

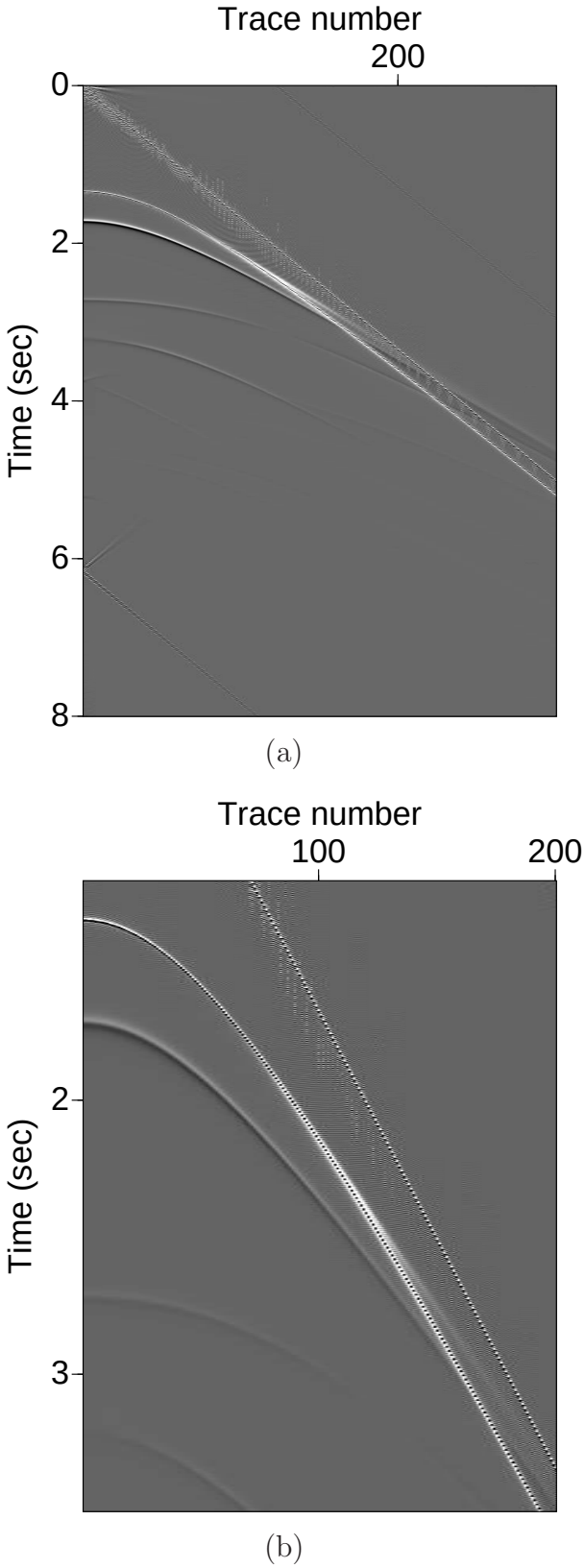

Figure 4. (a) Shot gather computed for the model in Figure 3 and (b) its blow-up showing reflections with different frequency content.

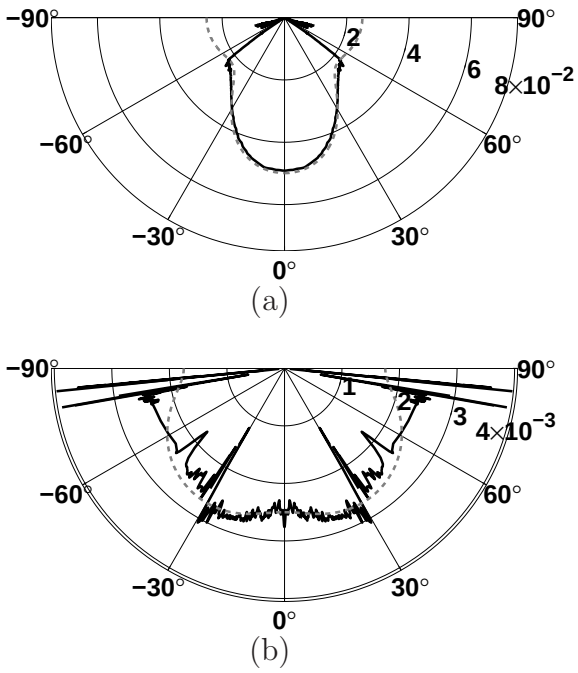

Figure 5. Normalized interval phase attenuation coefficient $\mathcal{A}$ (solid black lines) for the second (a) and third (b) layers of the model from Figure 3 computed as a function of phase angle. The dashed gray lines mark the exact values of $\mathcal{A}$.

(Zhu & Tsvankin, 2006):

$$\mathcal{A} \quad = \quad \mathcal{A}_{P0}\left(1+\delta_{_Q}\sin^2\theta\,\cos^2\theta+\epsilon_{_Q}\sin^4\theta\right), \qquad (10)$$

where θ is the phase angle with the symmetry axis.

5 CONCLUSIONS

We extended velocity-independent layer stripping to amplitude analysis and employed the spectral-ratio method to obtain the interval attenuation coefficient from reflection data. While the target layer can be arbitrarily anisotropic and heterogeneous, the overburden has to be laterally homogeneous with a horizontal symmetry plane. It should be emphasized that our attenuation layer stripping does not require knowledge of the overburden velocity and attenuation parameters.

Numerical examples for layered VTI media confirm that the method yields accurate interval phase attenuation coefficients even for models with uncommonly strong attenuation and substantial velocity and attenuation anisotropy. The algorithm is designed to process isolated overburden and target reflections, so the results may be distorted by interference with other events. As any other layer-stripping technique, our method may become inaccurate for thin attenuative layers.

Interval attenuation measurements may provide important information for reservoir characterization and monitoring. The 3D version of the method can be used to estimate azimuthally varying interval attenuation coefficients for fracture-characterization purposes.

ACKNOWLEDGMENTS

We are grateful to the members of the A(nisotropy)-Team of the Center for Wave Phenomena (CWP), Colorado School of Mines for helpful discussions. Support for this work was provided by the Consortium Project on Seismic Inverse Methods for Complex Structures at CWP and the Petroleum Research Fund of the American Chemical Society. We thank Subhashis Mallick (Chevron ETC) for help with synthetic modeling. The synthetic data were generated using the reflectivity code OASES (courtesy of MIT).

References

Batzle, M. L., Han, De-H., & Hofmann, R. 2006. Fluid mobility and frequency-dependent seismic velocity — Direct measurements. *Geophysics*, **71**, N1–N9.

Behura, J., Batzle, M., & Hofmann, R. 2006. Shear properties of oil shales. *SEG Technical Program Expanded Abstracts*, **25**(1), 1973–1977.

Behura, J., Batzle, M., Hofmann, R., & Dorgan, J. 2007. Heavy oils: Their shear story. *Geophysics*, **72**(5), E175–E183.

Dasgupta, R., & Clark, R. A. 1998. Estimation of Q from surface seismic reflection data. *Geophysics*, **63**(6), 2120–2128.

Dewangan, P., & Tsvankin, I. 2006. Velocity-independent layer stripping of PP and PS reflection traveltimes. *Geophysics*, **71**(4), U59–U65.

Ganley, D. C., & Kanasewich, E. R. 1980. Measurement of absorption and dispersion from check shot surveys. *Journal of Geophysical Research*, **85**(Oct.), 5219–5226.

Hosten, B., Deschamps, M., & Tittmann, B. R. 1987. Inhomogeneous wave generation and propagation in lossy anisotropic solids - Application to the characterization of viscoelastic composite materials. *Acoustical Society of America Journal*, **82**(Nov.), 1763–1770.

Liu, E., Chapman, M., Varela, I., Li, X., Queen, J. H., & Lynn, H. 2007. Velocity and attenuation anisotropy: Implication of seismic fracture characterizations. *The Leading Edge*, **26**, 1170–1174.

Maultzsch, S., Chapman, M., Liu, E., & Li, X. 2007. Modelling and analysis of attenuation anisotropy in multi-azimuth VSP data from the Clair field. *Geophysical Prospecting*, **55**, 627–642.

Prasad, M., & Nur, A. 2003. Velocity and attenuation anisotropy in reservoir rocks. *SEG Technical Program Expanded Abstracts*, **22**, 1652–1655.

Tao, G., & King, M. S. 1990. Shear-wave velocity and

Q anisotropy in rocks: A laboratory study. *International Journal of Rock Mechanics and Mining Science & Geomechanics Abstracts*, **27**(Oct.), 353–361.

Vasconcelos, I., & Jenner, E. 2005. Estimation of azimuthally varying attenuation from wide-azimuth P-wave data. *SEG Technical Program Expanded Abstracts*, **24**, 123–126.

Winkler, K. W., & Nur, A. 1982. Seismic attenuation: Effects of pore fluids and frictional-sliding. *Geophysics*, **47**, 1–15.

Zhu, Y. 2006. *Seismic wave propagation in attenuative anisotropic media.* Ph.D. thesis, Colorado School of Mines.

Zhu, Y., & Tsvankin, I. 2006. Plane-wave propagation in attenuative transversely isotropic media. *Geophysics*, **71**(2), T17–T30.

Zhu, Y., Tsvankin, I., Dewangan, P., & van Wijk, K. 2007. Physical modeling and analysis of P-wave attenuation anisotropy in transversely isotropic media. *Geophysics*, **72**(1), D1–D7.